CVR-2019-0975

RyR2 regulates Cx43 hemichannel intracellular Ca^{2+}-dependent activation in cardiomyocytes

Alessio Lissoni[1], Paco Hulpiau[2], Tânia Martins-Marques[3], Nan Wang[1], Geert Bultynck[4], Rainer Schulz[5], Katja Witschas[1], Henrique Girao[3], Maarten De Smet[1,6#] and Luc Leybaert[1#^]

[1] *Department of Basic And Applied Medical Sciences – Physiology group, Ghent University, Ghent 9000, Belgium*
[2] *HOWEST University of Applied Sciences (Hogeschool West-Vlaanderen), Bruges, Belgium*
[3] *Coimbra Institute for Clinical and Biomedical Research (iCBR), Faculty of Medicine, University of Coimbra, 3000-354 Coimbra, Portugal*
[4] *Department of Molecular Cell Biology, Laboratory of Molecular and Cellular Signaling, KU Leuven, Leuven, Belgium*
[5] *Institut für Physiologie, JustusLiebig Universität Giessen, Giessen, Germany*
[6] *Department of Internal Medicine, Ghent University, Ghent, Belgium*

[#] both authors share senior authorship
^Corresponding author

Short title: Caffeine-triggered Cx43 hemichannel opening in the heart.

Author Contribution

A. Lissoni, M. De Smet and L. Leybaert conceived the study; A. Lissoni carried out the experiments and the data analysis; P. Hulpiau performed the docking study and prepared the related figure and text; T. Martins-Marques and H. Girao provided the Co-IP data and prepared the related figure and text; N. Wang contributed to the design of the experiments; G. Bultynck helped in interpreting the docking study; R. Schulz conceived the global inducible Cx43 knockdown experiments and supervised analysis and interpretation; K. Witschas and M. De Smet guided the patch-clamp data analysis and interpretation; A. Lissoni wrote the manuscript in consultation with L. Leybaert who supervised the project. All authors discussed the results and contributed to the final manuscript.

Category of the manuscript: Original article
Total word count of the manuscript: 8481

Abstract:

Aims:
Connexin-based gap junctions are crucial for electrical communication in the heart; they are each composed of two docked hemichannels, supplied as unpaired channels via the sarcolemma. When open, an unpaired hemichannel forms a large pore, high-conductance and Ca^{2+}-permeable membrane shunt pathway that may disturb cardiomyocyte function. Hemichannels composed of connexin43, a major cardiac connexin, can be opened by electrical stimulation but only by very positive membrane potentials. Here, we investigated the activation of connexin43 hemichannels in murine ventricular cardiomyocytes voltage-clamped at -70 mV.

Methods and Results:
Using whole-cell patch clamp, Co-IP, Western blot analysis, immunocytochemistry, proximity ligation assays and protein docking studies, we found that stimulation of ryanodine receptors (RyRs) triggered unitary currents with a single-channel conductance of ~220 pS, which were strongly reduced by connexin43 knock-down. Recordings under Ca^{2+}-clamp conditions showed that both RyR activation and intracellular Ca^{2+} elevation were necessary for hemichannel opening. Proximity ligation studies indicated close connexin43-RyR2 apposition (<40 nm), and both proteins co-immunoprecipitated indicating physical interaction. Molecular modeling suggested a strongly conserved RyR-mimicking peptide sequence (RyRHCIp), which inhibited RyR/Ca^{2+} hemichannel activation but not voltage-triggered activation. The peptide also slowed down action potential repolarization.

Conclusions:
Our results demonstrate that connexin43 hemichannels are intimately linked to RyRs, allowing them to open at negative diastolic membrane potential in response to RyR activation.

Translational Perspective:

We here provide detailed evidence that Cx43 hemichannels can be opened by concomitant RyR activation and $[Ca^{2+}]_i$ elevation, two fundamental players in cardiomyocyte excitation-contraction coupling. Recent work in a plakophillin-2 deficient mouse model for ARVC indicated RyR2-linked Ca^{2+} dysregulations that were suppressed by the Cx43 hemichannel inhibitor Gap19. Our present work delineates the necessary conditions to activate Cx43 hemichannels in RyR2- and Ca^{2+}-dependent manners and provides a new peptide tool, RyRHCIp, that inhibits hemichannel opening by acting at this crucial RyR-hemichannel axis.

1. Introduction:

Connexin 43 is the most abundant connexin isotype in the heart. It is most prominently located at the level of the intercalated discs (IDs) of cardiomyocytes where it forms GJs [1]. GJ channels are formed by the docking of two hemichannels (HCs) and given the high Cx43 turnover rate, this necessitates continuous supply of HCs through the perinexal area adjacent to the gap junctional plaques [1–3]. While GJs are normally open, HCs are closed under resting conditions; Cx43-based HCs open in response to various conditions including metabolic inhibition [4,5], voltage steps to positive membrane potential [6,7], alterations in the phosphorylation and redox status [8–11], low extracellular Ca^{2+} [12,13], or an increase in intracellular calcium concentration ($[Ca^{2+}]_i$) [7,14–16]. Importantly, HC opening in response to $[Ca^{2+}]_i$ elevation has only been documented by non-electrophysiological methods such as ATP release or dye uptake hemichannel assays, except for astrocytes where electrophysiological evidence is available [17]. In cardiomyocytes, we previously demonstrated that Cx43 HC opening triggered by electrical stimulation to positive voltages is modulated by $[Ca^{2+}]_i$ elevation, which lowers the voltage threshold for activation [7]. However, the activation voltage threshold remains high (+40 mV) and needs to be maintained for a sufficient period, leaving the question open whether such conditions can be realistically achieved during the cardiac action potential. Nothing is currently known concerning HC activation at negative diastolic membrane potentials and we thus aimed to investigate conditions under which $[Ca^{2+}]_i$ elevation could directly trigger Cx43 HC opening in cardiomyocytes.
When open, Cx43 HCs behave as poorly selective channels, with a large pore characterized by a unitary conductance of ~220 pS, allowing transmembrane exchange of ions and small molecules that may affect electrochemical and metabolic cell homeostasis [7,14,18]. Connexinopathies involving Cx43 have been related to several cardiac diseases, such as sudden death, myocardial ischemia, ventricular arrhythmia, ventricular hypertrophy and recently to arrhythmogenic right ventricular cardiomyopathy (ARVC) [19–23], in most cases linked to altered gap junctional electrical conduction. Here, we combined single channel electrophysiological approaches and molecular modeling to investigate conditions and mechanisms leading to Cx43 HC opening in acutely isolated ventricular cardiomyocytes. While previous work showed that Cx43 HC opening could only be induced by strongly positive membrane potentials [7,24], we now demonstrate in cardiomyocytes held at normal negative resting potential that Cx43 HCs can be opened by moderate $[Ca^{2+}]_i$ elevation when combined with activation of RyRs as e.g. by caffeine. Co-immunoprecipitation as well as proximity ligation assays suggested interaction between Cx43 and RyR2, which was further pinned down by molecular modeling to a short amino acid sequence on the P1 domain of type 2 RyRs and the C-terminal tail of Cx43. RyRHCIp, identical to the predicted RyR2 interaction site, inhibited the combined $[Ca^{2+}]_i$ elevation/RyR2 activation-induced HC opening, while scrambled RyRHCIp had no effect.

2. Material and Methods:

An expanded Methods section is available in the Supplementary material online.

2.1 Cardiomyocyte isolation

Animal handling and procedures were approved by the Committee on ethical usage of animals of Ghent University and conformed to directive 2010/63/EU of the European Parliament.

Adult C57BL6 mice, between 10 - 16 weeks, were heparinized (5000 IU/kg IP) and sacrificed by cervical dislocation. Following thoracotomy, the heart was quickly excised and then transferred to a Langendorff apparatus and perfused at a constant flow (~3 mL/min) and temperature (37°C). The heart was digested using collagenase and protease and left ventricular isolated cardiomyocytes were collected. Ca^{2+}-tolerant cells were used for the experiment for the next 6 hours.
In case of Cx43 knockdown (KD) ($Cx43^{CreER(T)/fl}$) and respective control mice ($Cre43^{fl/fl}$) the isolation procedures were preceded by daily injection of tamoxifen to achieve global knockdown condition [25].

2.2 Hela cell culture

HeLa Cells (up to passage 16) stably transfected with Cx43 (HeLa Cx43, [26]), were maintained in Dulbecco's modified Eagle's medium (Invitrogen, Gent, Belgium) and incubated at 37°C and 10 % CO_2.

2.3 Immunocytochemistry and colocalization analysis

Colocalization analysis was performed on acute isolated mouse ventricular cardiomyocytes. The cells were stained with rabbit anti-Cx43 (Sigma-Aldrich, Cat no. C6219) and mouse anti-RyR C3-33 (Thermo Scientific, Cat no. MA3-916). Afterwards, confocal imaging was performed using a Leica XPS-8 with a water emersion objective 63X (numerical aperture 1.2). The Manders coefficient was used to quantify the degree of colocalization [27].

2.4 Proximity Ligation Assay

Adult C57BL6 mice were sacrificed as describe above and hearts were embedded in OCT medium (Klinipath) and then cut using a cryostat at 3 µm thickness. Proximity ligation was done on mouse ventricular slices according to manufacturer protocol (Sigma-Aldrich, Duolink kit DUO92101) to detect Cx43/RyR2 proximity. Rabbit anti-Cx43 (Sigma-Aldrich, Cat no. C6219) and mouse anti-RyR C3-33 (Thermo Scientific, Cat no. MA3-916) were used as primary antibodies. For the positive controls, we used mouse anti-Cx43 clone 4E6.2 (MerckMillipore, Cat no. MAB3067) and rabbit anti-Cx43.

2.5 Western blot analysis

For Western blots, heart tissue samples collected during cardiomyocyte isolation were lysed and proteins were resolved in 4–12 % Bis-Tris gels (Invitrogen) and transferred to a nitrocellulose membrane (Amersham, Buckinghamshire, UK). Blots were probed with a rabbit anti-Cx43 antibody (Sigma-Aldrich) followed by alkaline phosphatase-conjugated goat anti-rabbit IgG antibody (Sigma-Aldrich). The blots were then developed with nitro blue tetrazolium/5-bromo-4-chloro-3-indolyl-phosphate reagent (Zymed, Invitrogen). Total protein stains by SYPRO Ruby (Invitrogen) prior to antibody staining was used as a loading control. Quantification was performed by using ImageJ.

2.6 Immunoprecipitation assay

Co-immunoprecipitation (Co-IP) experiments were performed as described previously [28]. Lysates from both mouse whole hearts and isolated ventricular cardiomyocytes were prepared in lysis buffer. Determination of total protein was performed by the DC Protein Assay (BioRad, Hercules, CA), after which 1 mg of the supernatants were used for immunopurification. Proteins were resolved in 8% SDS-poly-acrylamide (SDS-PAGE) gel and transferred to a nitrocellulose membrane (BioRad, Hercules, CA). Blots were probed with primary antibodies against RyR2 (C3-33, Sigma-Aldrich), N-cadherin (H-63, sc-7939; Santa Cruz Biotechnology, Heidelberg, Germany), Cx43 (AB0016) and Calnexin (AB0041, Sicgen), followed by appropriate horseradish peroxidase-conjugated IgG antibodies (BioRad). The proteins of interest were visualized by chemiluminescence using a VersaDoc system (Bio-Rad).

2.7 Modeling and Docking

To predict putative interactions between the mouse RyR2 and the Cx43 hemichannel (Gja1) homology modeling and docking studies were performed. A homology model of mouse RyR2 was built with Modeller [29]. The model of mouse RyR2 cytoplasmic domain and carboxy-terminal domain of Cx43 were used for docking by ClusPro [30] to predict binding of Cx43 to mouse RyR2. Homology and docking results were analyzed and figures were rendered using PyMOL.

2.8 Electrophysiological recording and intracellular calcium recording

Isolated ventricular cardiomyocytes and HeLa-Cx43 cells were studied under whole cell voltage-clamp to record membrane currents. Details of solution compositions, voltage protocols and current analysis are provided in the Supplementary material. Patch clamp experiments were conducted at room temperature (22 ± 1 ^{o}C).
Fluo-4 (25 µM) was used to detect the $[Ca^{2+}]_i$ transients during the current recording.

2.9 Statistical analysis

Data are expressed as mean ± s.e.m with n giving the number of cells and N giving the number of independent experiments. Two groups were compared with a paired or unpaired Student's t-test and two-tail P value depending on the experiment design. Multiple groups were compared by one-way analysis of variance and a Bonferroni posttest, making use of OriginLab software (OriginLab Corporation, USA). Results were considered statistically significant when $P< 0.05$ (* for $P < 0.05$, ** for $P < 0.01$, *** for $P < 0.001$ and **** for $P < 0.0001$).

3. Results:

3.1 RyR agonists trigger unitary current activity with properties that resemble Cx43 HC opening

We used two different RyR agonists, caffeine (10 mM) and 4-cmc (1 mM) [31], to trigger currents recorded in whole cell mode from acutely isolated mouse ventricular cardiomyocytes voltage-clamped at a holding potential of -70 mV. Recordings were done in extracellular normal-Tyrode and intracellular KAsp based solutions (see Materials and methods). Caffeine (8 s) triggered a large inward current followed by a recovery phase that is known to be mediated by Na^{+}/Ca^{2+} exchange (NCX) in

response to the caffeine-triggered sarcoplasmic reticulum (SR) Ca^{2+} release [32] (Fig. 1a upper panel). Superimposed on this macroscopic current were small spiking inward currents that appeared with a grossly similar amplitude. After subtraction of the NCX current (Fig. 1a, red trace) these unitary events were more easily appreciated and all-events histogram analysis indicated a unitary conductance of ~220 pS (assuming ~0 mV reversal potential, confirmed in Fig. 2g), typical of Cx43 HCs [7] (Fig. 1b upper panel). The macroscopic NCX-based current triggered by 4-cmc was somewhat different (multiphasic) from the caffeine-triggered one, but the unitary current events had similar properties as those observed with caffeine (Fig. 1a, b lower panels). Cx43 HCs can be opened by modest $[Ca^{2+}]_i$ elevation in voltage-clamped astrocytes held at -70 mV [17] and RyR-triggered $[Ca^{2+}]_i$ elevation in response to caffeine/4-cmc may thus play a role in the presently observed unitary current activities. To investigate whether $[Ca^{2+}]_i$ elevation by itself is sufficient to trigger unitary events, we performed experiments without caffeine or 4-cmc and applied low extracellular Na^+ (1 mM) to reverse the NCX working mode and let it pump in Ca^{2+} to obtain $[Ca^{2+}]_i$ elevation [33]. Ryanodine (100 µM) was included in the pipette solution to avoid Ca^{2+}-induced Ca^{2+} release [34,35] (Fig. 1c). In contrast to the caffeine/4-cmc experiments, no unitary current events were observed under those conditions (Fig. 1d), suggesting that $[Ca^{2+}]_i$ elevation alone is not sufficient to elicit Cx43 HC opening.

3.2 Combined RyR activation/$[Ca^{2+}]_i$ elevation is necessary to trigger unitary current activity

Caffeine/4-cmc triggers two combined events, RyR activation and subsequent $[Ca^{2+}]_i$ elevation, and we next aimed to separate both processes. To that purpose, we used a strongly Ca^{2+}-buffered pipette solution containing 10 mM BAPTA to clamp $[Ca^{2+}]_i$ to 50 (resting condition), 250, 500 and 1000 nM. These calculated $[Ca^{2+}]_i$ values were verified by ratiometric fura-2 measurements, which resulted in actual Ca^{2+} concentrations of 49 ± 2, 283 ± 11, 505 ± 16 and 781 ± 25 nM (N = 3) respectively. For simplicity, we further refer to the calculated concentrations in the following text. Fig. 2a illustrates a current trace recorded with the normal pipette solution without added BAPTA (V_m = -70 mV), demonstrating that the first caffeine application triggered a large inward current with superimposed unitary current activity. However, the second caffeine application did not trigger any unitary current activity, indicating SR Ca^{2+} store depletion. By contrast, recordings with $[Ca^{2+}]_i$ clamped to 250 nM showed quite different responses (Fig. 2b). First, caffeine application did not trigger any NCX current, which is considered to be a reliable reporter of $[Ca^{2+}]_i$ in the subsarcolemmal compartment [36–38], indicating that $[Ca^{2+}]_i$ is well clamped and stable. Second, unitary current activity was triggered not only by the first, but also by the second caffeine application, indicating that the $[Ca^{2+}]_i$ imposed via the pipette is sufficient and SR Ca^{2+} release is not necessary. In line with this, the RyR inhibitors ryanodine and dantrolene [34,39,40] did not inhibit caffeine-induced Cx43 HC activation (supplementary Fig. S1a). Importantly, in between the two caffeine applications no unitary events occurred with 250 nM $[Ca^{2+}]_i$ demonstrating that both $[Ca^{2+}]_i$ elevation and caffeine activation of RyRs are necessary for triggering unitary activity. Fig. 2c illustrates experiments with simultaneous fluo-4 (25 µM in the pipette solution) recording of $[Ca^{2+}]_i$, demonstrating absence of unitary events when caffeine challenges were applied at resting $[Ca^{2+}]_i$ of 50 nM [41] and appearance of unitary activities with caffeine applied at higher $[Ca^{2+}]_i$. As was already clear from the absence of NCX currents, the fluo-4 recordings were stable during caffeine applications confirming stable $[Ca^{2+}]_i$ clamp. Histogram analysis showed a conductance peak at ~ 220 pS (225 ± 5 pS) in the 250 nM $[Ca^{2+}]_i$ condition, while double and triple stacked openings superimposed on each other were present mostly at 500 nM $[Ca^{2+}]_i$ were the Cx43 HC activity was higher (Fig. 2d). Average charge transfer (Q_m) data of these experiments are shown in Fig. 2e, demonstrating a two-phased $[Ca^{2+}]_i$ modulation of HC activity with $[Ca^{2+}]_i$ below ~500 nM activating HC opening and concentrations above ~500 nM reducing HC

activity. The activation has been linked to calmodulin-dependent signaling [14], while the limiting effect is, based on evidence obtained in non-muscle cells, the result of actomyosin contractility and disruption of Cx43 cytoplasmic loop/C-terminal tail interactions, which are necessary for HC opening [16,42]. Thus, Cx43 HCs can be opened by combined RyR/$[Ca^{2+}]_i$ activation, but opening is counteracted when $[Ca^{2+}]_i$ becomes too high.

We further explored the voltage dependence of the unitary current activities at 250 nM $[Ca^{2+}]_i$ for different potentials and found a switch from fast spiking events at negative potential to long-lasting openings at positive potentials (Fig. 2f); the latter were identical to those described previously for pure voltage-triggered Cx43 HC openings [7]. Interestingly, at positive voltage (+20 and +30 mV) caffeine was not necessary to obtain HC opening (Supplementary Fig. S1b) while it was indispensable to trigger HC opening at -70 mV (Fig. 2b). Graphical representation of these distinct opening responses demonstrated a linear I-V relationship characterized by a reversal potential of ~0 mV and a slope conductance of 230 ± 2.8 pS (n = 10) (Fig. 2g), which is in line with the histogram-based conductance analysis at -70 mV. The 230 pS conductance significantly differs from the 300-400 pS RyR or polycystin-2-like channel conductance that has previously been proposed to mediate sarcolemmal caffeine-triggered spiking inward currents [43]; it also differs from the Panx1 channel conductance reported to contribute to caffeine-triggered spiking current activity in atrial cells [44]. Our data show RyR activation combined with $[Ca^{2+}]_i$ elevation is necessary to activate Cx43 HC spiking inward current activity at -70 mV.

3.3 Unitary current activity triggered by combined RyR/$[Ca^{2+}]_i$ activation is strongly reduced in cardiomyocytes isolated from Cx43 knockdown animals

We determined whether the unitary event activity was dependent on Cx43 expression and applied the combined 250 nM $[Ca^{2+}]_i$/caffeine activation protocol on cardiomyocytes isolated from inducible global Cx43 knockdown animals. Fig. 3a shows typical current traces recorded in $Cx43^{fl/fl}$ control mice and $Cx43^{Cre\text{-}ER(T)/fl}$ tamoxifen-inducible Cx43 knockdown mice; both strains received tamoxifen (see materials and methods) and Fig. 3c summarizes average data of these experiments. Charge transfer related to unitary current activity was on average 4-fold lower in $Cx43^{Cre\text{-}ER(T)/fl}$ mice compared to $Cx43^{fl/fl}$ mice. Western blot analysis of Cx43 expression in ventricular heart lysates showed a ~10-fold decrease of Cx43 in $Cx43^{Cre\text{-}ER(T)/fl}$ relative to $Cx43^{fl/fl}$ animals (Fig. 3b). Taken together, these experiments demonstrate that the unitary event activity triggered by combined RyR activation/$[Ca^{2+}]_i$ elevation is largely mediated by Cx43 HCs. As a control experiment, we tested whether the strongly decreased Cx43 expression in $Cx43^{Cre\text{-}ER(T)/fl}$-derived cardiomyocytes influenced the action potential properties in ventricular cardiomyocytes. We found a shorter APD_{50} compared to control mice (Table 1; Fig. 6f), shown previously to be linked to remodeling of K^+ inward rectifier (I_{K1}), L-type Ca^{2+} and Nav1.5 channels [45].

3.4 Cx43 interacts with RyR2 at the level of the intercalated disc

Since co-activation of RyRs is necessary to trigger Cx43 HC opening by $[Ca^{2+}]_i$ elevation, we verified whether an interaction between the two proteins is necessary. Cardiomyocytes express both RyR1 and RyR2 isoforms; RyR1 is found at mitochondria [46–48] or at IDs [49]. We here focused on RyR2 as the most prevalent isoform in cardiac tissue [50,51] and used an antibody strongly reactive for the RyR2 isoform.

We first investigated *in situ* co-localization of Cx43 and RyR2, and then attempted to detect physical interactions between both proteins in ventricular cardiomyocytes. Fig. 4a illustrates double label

immunofluorescence microscopy images of acutely isolated ventricular cardiomyocytes, indicating that ~24 % of the Cx43 signal co-localized with the RyR2 signal at the level of the ID. Fig. 4b illustrates the tissue organization of RyR2 and Cx43, with the latter being located at the junctional area between adjacent cardiomyocytes [2,3,52]. Proximity ligation DuoLink studies targeting Cx43 and RyR2 showed positive signals between Cx43 and RyR2 at the IDs counterstained by pan-Cadherin immunostaining, suggesting apposition of the two proteins within less than 40 nm (Fig. 4b). As a positive control condition, we tested two different Cx43 antibodies recognizing distinct epitopes (Fig. 4c) and found a typical ID-located distribution of the DuoLink signal. Negative control experiments performed by omitting one of the primary antibodies gave no DuoLink signal (Supplementary Fig. S2). To complement the immunochemistry-based approaches, we further assessed interactions between Cx43 and RyR2 by co-immunoprecipitation assays of protein from mouse adult heart lysates. These experiments demonstrated that RyR2 and N-cadherin co-precipitated with Cx43, both in whole heart lysates (Fig. 5a left) and lysates isolated from ventricular cardiomyocytes (Fig. 5a right) [28]. Overall these results strongly suggest a direct protein-protein interaction between Cx43 and RyR2 at ID-located areas in mouse cardiomyocytes.

3.5 The RyR2 mimetic peptide RyRHCIp inhibits Cx43 hemichannel opening induced by combined RyR/$[Ca^{2+}]_i$ activation

The interaction between Cx43 and RyR2 was further investigated using ClusPro web server for protein-protein docking analysis (see Material and Methods). For this study, a mouse RyR2 model based on the homotetrameric rabbit RyR1 3J8H (Fig. 5b [53]), and an NMR-based reconstruction of the C-terminal domain of Cx43 were used [54]. Following several simulation rounds, a common cluster region was identified between the P1 domain of RyR2 (sequence KNRRNPRL) and a corresponding interacting string on Cx43 located at the level of the second alpha helix of the CT domain (sequence FDFPDDN; Fig. 5c), involving several electrostatic interactions. The RyR2 sequence KNRRNPRLVPY, part of the RyR2 P1 domain, is fully conserved in human, mice, rat, chicken and several other species (supplementary Fig. S4). Modification of the second Arg in this sequence to Lys (Arg1027Lys) is phenotypically associated with primary familial hypertrophic cardiomyopathy. The RNPRL part of the sequence is furthermore conserved in RyR1. Along the same line, the interacting FDFPDDN sequence on the Cx43 protein is also well conserved.

Based on these data, we synthetized an 11 amino acid RyR2 mimetic peptide, further called RyRHCIp, that contained the predicted sequence with an additional 3 more residues at its C-terminal end to increase binding selectivity (KNRRNPRLVPY), and subsequently tested its effect on Cx43 HC opening induced by $[Ca^{2+}]_i$ elevation/RyR activation. RyRHCIp (250 µM) was included in the 250 nM $[Ca^{2+}]_i$ pipette solution, allowed to equilibrate for 2 minutes after breaking into the cell and followed by repetitive assessment of Cx43 HC activity every 30 sec. Fig. 6a-b shows the effect of the peptide compared to its scrambled version (ScrRyRHCIp) and the control condition without peptide. RyRHCIp significantly inhibited Cx43 HC opening within 2 min, while ScrRyRHCIp as well as the control condition had no effect, as illustrated in the Q_m plots.

We next verified whether RyRHCIp would also affect HC activity in HeLa cells stably transfected with Cx43, which endogenously express RyR2 [55], but lack the typical ventricular cardiomyocyte sarcolemmal organization. As a first experiment we tested whether caffeine (10 mM) could trigger spiking unitary HC current activity at negative potential, as observed in the preceding ventricular cardiomyocytes experiments, but this was not the case (see supplementary Fig. S3). Subsequently, we elicited HC opening by voltage steps to positive V_m (+70 mV), and set $[Ca^{2+}]_i$ to 250 nM to enhance

electrically-triggered HC opening [7]. Fig. 6c shows representative Cx43 HC current traces and corresponding all-point histograms demonstrating ~220 pS unitary event activity (Fig. 6d). Summary Q_m data presented in Fig. 6e demonstrate that RyRHCIp had no inhibitory effect on HC currents activated by voltage steps to positive potentials. Taken together, the spiking mode of HC activation at -70 mV is only observed in ventricular cardiomyocytes endowed with the necessary cytoarchitectural organization of RyR and Cx43 proteins, and RyRHCIp only affects HC activity induced by combined RyR/$[Ca^{2+}]_i$ activation, i.e. chemically activated HC opening, while not affecting electrically-triggered HC opening; Table 2 summarizes the differences between these two modes of Cx43 HC activation. In the last experiment we further tested whether RyRHCIp would affect the action potential properties in cardiomyocytes and found the peptide to elongate the APD_{90} (Table 1; Fig. 6f).

4. Discussion:

Besides the canonical role of connexins in GJs, evidence is accruing that normally closed HCs may open under certain conditions [3–5]. Previous studies demonstrated Cx43 HC activity in cardiomyocytes in response to positive membrane voltages equal to or larger than +40 mV [7]. Here we describe Cx43 HC opening at negative diastolic membrane potential upon challenging ventricular cardiomyocytes with combined RyR/$[Ca^{2+}]_i$ activation (Fig. 2b-c). Comparable caffeine-triggered fast spiking channel activity has been reported in cardiomyocytes by others[56–58], but the single channel conductances were different (RyR, polycystin-2-like channels) from those reported here, were found in atrial cardiomyocytes (Panx1) or would suffice caffeine stimulation without associated $[Ca^{2+}]_i$ elevation (sarcolemmal RyRs). $[Ca^{2+}]_i$ activation of Cx43 HCs occurs in a physiological range, up to 500 nM $[Ca^{2+}]_i$, while opening is tempered at higher concentrations and largely decreased at ~800 nM (Fig. 2c-e). Previous work in cardiomyocytes showed that electrically activated HC openings can be modulated but not triggered by $[Ca^{2+}]_i$ elevation [7]. Interestingly, combined RyR/$[Ca^{2+}]_i$-triggered Cx43 HC openings at negative membrane potential are very brief (9.02 ± 0.36 msec, n = 869; N = 5) compared to the long openings observed with electrical stimulation at positive voltage, which may last for hundreds of milliseconds (Fig. 2f-g). This suggests that the $[Ca^{2+}]_i$-based trigger, which involves calmodulin signaling [7], activates gating elements that behave differently from those activated by positive voltages. We found that $[Ca^{2+}]_i$ elevations alone were not sufficient to elicit Cx43 HC opening, but required simultaneous RyR activation (Fig. 2b-e). Interestingly, RyR2 and Cx43 co-immunoprecipitated (Fig. 5a) and co-localized within less than 40 nm at the level of IDs (Fig. 4a-b). Such Cx43-RyR2 interaction has been demonstrated to be involved in cardiac ischemia-reperfusion injury [28]. Using a bioinformatics approach, we identified putative RyR2-Cx43 interaction sequences on both proteins, located in the P1 domain of RyR2 and the CT domain of Cx43 (Fig. 5b,c). The predicted Cx43 interaction site partially overlaps with the second alpha helical region of Cx43 that has previously been suggested to affect chemically-induced Cx43 channel gating via CT-CL (loop-tail) interaction [59]. The concerned Cx43 interaction site is largely unexplored in terms of its role in channel/hemichannel function [60]; our data demonstrate involvement of this interaction site in RyR-linked Ca^{2+} activation of Cx43 HCs. RyRHCIp, which contains the sequence of the predicted P1 domain on RyR2, inhibited the combined RyR/$[Ca^{2+}]_i$-triggered opening of Cx43 HCs (Fig. 6a,b). Molecular modeling suggests that RyRHCIp interacts with the Cx43-located ^{335}FDFPDDN^{341} sequence, rendering it inaccessible for RyR2-linked HC activation. The fact that RyRHCIp did not affect HC opening in HeLa-Cx43 cells (Fig. 6c-e), which also express RyR2 [55], is an interesting observation that needs to be further scrutinized in other non-cardiac cells for potential RyRHCIp effects outside the heart. The mechanism of how RyR2 activation facilitates HC opening is currently not clear. Of note, Cx43 HCs necessitate loop-tail (CL-CT) interaction for opening [16,61], (reviewed in

[60]). As such, we anticipate that RyR2 activation with caffeine/4-cmc may favor Cx43 loop-tail interactions through the predicted RyR2-Cx43 linkage. This would bring the Cx43 protein into a state where HCs become available to open when a trigger condition is present (Fig. 7). Our experiments suggest that $[Ca^{2+}]_i$-elevation acts as the additional signal effectively opening HCs from this available to open state.
In terms of electrical effects, RyRHCIp increased the APD_{90} in a way that is similar to observations in conditional Cx43D378stop mice, which lack the last 5 CT amino acids [62]. The latter domain is, like the presently proposed second alpha helical CT domain, involved in Cx43 HC gating [24,59]. Given the fact that Cx43 is, in addition to its channel functions, also a major signaling hub for many proteins, it is likely that this RyRHCIp effect may involve interaction at the protein level as well.

In conclusion, our data provide the first detailed evidence in ventricular cardiomyocytes that Cx43 HCs can be opened at negative diastolic membrane potential, by concomitant RyR activation and $[Ca^{2+}]_i$ elevation. Intracellular Ca^{2+} and RyR are two fundamental factors involved in the excitation-contraction signaling that leads to cardiac contraction. Caffeine challenging of RyRs is a common experimental procedure to induce pro-arrhythmogenic conditions whereby altered cardiomyocyte Ca^{2+} cycling and spontaneous SR Ca^{2+} release events are hallmark events [63–66]. Such events associated with diastolic $[Ca^{2+}]_i$ elevation typically occur in diastolic dysfunction [67], inherited RyR2 mutations [68] and tachycardia [69]. Recent work in a plakophillin-2 deficient mouse model for ARVC indicated RyR2-linked Ca^{2+} dysregulations that were suppressed by the Cx43 HC inhibitor Gap19 [23]. Our work delineates the necessary conditions to activate Cx43 HCs in RyR2- and Ca^{2+}-dependent manners and provides a new peptide tool, RyRHCIp, that inhibits HC opening by acting at this crucial RyR-HC axis.

Funding:

This work was supported by the Fund for Scientific Research Flanders, Belgium (G052718N to L. Leybaert) and Ghent University (BOF 01IO8314 to A. Lissoni). M. De Smet is supported by a personal grant from the Research Foundation Flanders (1124418N).

Acknowledgments:

We sincerely thank Dr. Ellen Cocquyt, Diego De Baere and Dr. Vicky Pauwelyn for superb technical support.
We are very grateful for the excellent advice and help we received from Prof. Karin Sipido (KULeuven, Belgium) regarding action potential recordings in isolated cardiomyocytes.

Conflict of interest:

A patent application is pending for intellectual property protection of some of the material presented in this study

References:

1. Delmar, M. & Liang, F.-X. Connexin43 and the regulation of intercalated disc function. *Hear.*

Rhythm **9,** 835–8 (2012).
2. Rhett, J. M., Jourdan, J. & Gourdie, R. G. Connexin 43 connexon to gap junction transition is regulated by zonula occludens-1. *Mol. Biol. Cell* **22,** 1516–28 (2011).
3. Rhett, J. M. & Gourdie, R. G. The perinexus: A new feature of Cx43 gap junction organization. *Hear. Rhythm* **9,** 619–623 (2012).
4. John, S. A., Kondo, R., Wang, S. Y., Goldhaber, J. I. & Weiss, J. N. Connexin-43 hemichannels opened by metabolic inhibition. *J. Biol. Chem.* **274,** 236–40 (1999).
5. Kondo, R. P., Wang, S.-Y., John, S. A., Weiss, J. N. & Goldhaber, J. I. Metabolic Inhibition Activates a Non-selective Current Through Connexin Hemichannels in Isolated Ventricular Myocytes. *J. Mol. Cell. Cardiol.* **32,** 1859–1872 (2000).
6. Contreras, J. E., Sáez, J. C., Bukauskas, F. F. & Bennett, M. V. L. Functioning of cx43 hemichannels demonstrated by single channel properties. *Cell Commun. Adhes.* **10,** 245–9 (2003).
7. Wang, N., De Bock, M., Antoons, G. K., Gadicherla, A., Bol, M., Decrock, E., Howard, E. W., Sipido, K., Bukauskas, F. & Leybaert, L. Connexin mimetic peptides inhibit Cx43 hemichannel opening triggered by voltage and intracellular Ca 2+ elevation. *Basic Res. Cardiol.* **107,** 1–17 (2012).
8. Retamal, M. A., Schalper, K. A., Shoji, K. F., Bennett, M. V. L. & Sáez, J. C. Opening of connexin 43 hemichannels is increased by lowering intracellular redox potential. *Proc. Natl. Acad. Sci. U. S. A.* **104,** 8322–7 (2007).
9. Bao, X., Reuss, L. & Altenberg, G. A. Regulation of purified and reconstituted connexin 43 hemichannels by protein kinase C-mediated phosphorylation of Serine 368. *J. Biol. Chem.* **279,** 20058–66 (2004).
10. Kim, D. Y., Kam, Y., Koo, S. K. & Joe, C. O. Gating connexin 43 channels reconstituted in lipid vesicles by mitogen-activated protein kinase phosphorylation. *J. Biol. Chem.* **274,** 5581–7 (1999).
11. Johnstone, S. R., Billaud, M., Lohman, A. W., Taddeo, E. P. & Isakson, B. E. Post-translational modifications in connexins and pannexins. *J. Membr. Biol.* **245,** 319–32 (2012).
12. Stout, C. & Charles, A. Modulation of Intercellular Calcium Signaling in Astrocytes by Extracellular Calcium and Magnesium. *Glia. 265-73.* **43,** (2003).
13. Stout, C. E., Costantin, J. L., Naus, C. C. G. & Charles, A. C. Intercellular Calcium Signaling in Astrocytes via ATP Release through Connexin Hemichannels. *J Biol Chem. (12)10482-8.* **277,** (2002).
14. De Vuyst, E., Wang, N., Decrock, E., De Bock, M., Vinken, M., Van Moorhem, M., Lai, C., Culot, M., Rogiers, V., Cecchelli, R., Naus, C. C., Evans, W. H. & Leybaert, L. Ca2+ regulation of connexin 43 hemichannels in C6 glioma and glial cells. *Cell Calcium* **46,** 176–187 (2009).
15. De Vuyst, E., Decrock, E., Cabooter, L., Dubyak, G. R., Naus, C. C., Evans, W. H. & Leybaert, L. Intracellular calcium changes trigger connexin 32 hemichannel opening. *EMBO J.* **25,** 34–44 (2006).
16. Ponsaerts, R., De Vuyst, E., Retamal, M., D'hondt, C., Vermeire, D., Wang, N., De Smedt, H., Zimmermann, P., Himpens, B., Vereecke, J., Leybaert, L. & Bultynck, G. Intramolecular loop/tail interactions are essential for connexin 43-hemichannel activity. *FASEB J.* **24,** 4378–4395 (2010).
17. Meunier, C., Wang, N., Yi, C., Dallerac, G., Ezan, P., Koulakoff, A., Leybaert, L. & Giaume, C. Contribution of astroglial Cx43 hemichannels to the modulation of glutamatergic currents by D-serine in the mouse prefrontal cortex. *J. Neurosci.* **37,** 2204–16 (2017).
18. Kang, J., Kang, N., Lovatt, D., Torres, A., Zhao, Z., Lin, J. & Nedergaard, M. Connexin 43 hemichannels are permeable to ATP. *J. Neurosci.* **28,** 4702–11 (2008).
19. Basheer, W. A., Harris, B. S., Mentrup, H. L., Abreha, M., Thames, E. L., Lea, J. B., Swing, D. A., Copeland, N. G., Jenkins, N. A., Price, R. L. & Matesic, L. E. Cardiomyocyte-specific overexpression of the ubiquitin ligase Wwp1 contributes to reduction in Connexin 43 and arrhythmogenesis. *J. Mol. Cell. Cardiol.* **88,** 1–13 (2015).
20. Leithe, E., Mesnil, M. & Aasen, T. The connexin 43 C-terminus: A tail of many tales. *Biochim. Biophys. Acta - Biomembr.* **1860,** 48–64 (2018).

21. García, I. E., Prado, P., Pupo, A., Jara, O., Rojas-Gómez, D., Mujica, P., Flores-Muñoz, C., González-Casanova, J., Soto-Riveros, C., Pinto, B. I., Retamal, M. A., González, C. & Martínez, A. D. Connexinopathies: a structural and functional glimpse. *BMC Cell Biol.* 17 Suppl 1 (2016).
22. Schulz, R., Görge, P. M., Görbe, A., Ferdinandy, P., Lampe, P. D. & Leybaert, L. Connexin 43 is an emerging therapeutic target in ischemia/reperfusion injury, cardioprotection and neuroprotection. *Pharmacol. Ther.* **153,** 90–106 (2015).
23. Kim, J.-C., Pérez-Hernández Duran, M., Alvarado, F. J., Maurya, S. R., Montnach, J., Yin, Y., Zhang, M., Lin, X., Vasquez, C., Heguy, A., Liang, F.-X., Woo, S.-H., Morley, G. E., Rothenberg, E., Lundby, A., Valdivia, H. H., Cerrone, M. & Delmar, M. Disruption of Ca 2+ i Homeostasis and Cx43 Hemichannel Function in the Right Ventricle Precedes Overt Arrhythmogenic Cardiomyopathy in PKP2-Deficient Mice . *Circulation* (2019). doi:10.1161/circulationaha.119.039710
24. Wang, N., Vuyst, E. De, Ponsaerts, R., Boengler, K., Palacios-prado, N., Lai, C. P., Bock, M. De, Decrock, E., Bol, M., Vinken, M., Tavernier, J., Evans, W. H., Naus, C. C., Bukauskas, F. F., Sipido, R., Heusch, G., Schulz, R., Bultynck, G. & Leybaert, L. Selective inhibition of Cx43 hemichannels by Gap19 and its impact on myocardial ischemia/reperfusion injury. *Basic Res Cardiol.* **108,** 1–26 (2013).
25. Boengler, K., Ruiz-Meana, M., Gent, S., Ungefug, E., Soetkamp, D., Miro-Casas, E., Cabestrero, A., Fernandez-Sanz, C., Semenzato, M., Lisa, F. Di, Rohrbach, S., Garcia-Dorado, D., Heusch, G. & Schulz, R. Mitochondrial connexin 43 impacts on respiratory complex I activity and mitochondrial oxygen consumption. *J Cell Mol Med.* **16,** (8):1649-55 (2012).
26. Elfgang, C., Eckert, R., Lichtenberg-Fraté, H., Butterweck, A., Traub, O., Klein, R. A., Hülser, D. F. & Willecke, K. Specific permeability and selective formation of gap junction channels in connexin-transfected HeLa cells. *J. Cell Biol.* **129,** 805–17 (1995).
27. Manders, E. M. M., Verbeek, F. J. & Aten, J. A. Measurement of co-localization of objects in dual-colour confocal images. *J. Microsc.* **169,** 375–382 (1993).
28. Martins-Marques, T., Anjo, S. I., Pereira, P., Manadas, B. & Girão, H. Interacting Network of the Gap Junction (GJ) Protein Connexin43 (Cx43) is Modulated by Ischemia and Reperfusion in the Heart. *Mol. Cell. Proteomics* **14,** 3040–55 (2015).
29. Webb, B. & Sali, A. Comparative Protein Structure Modeling Using MODELLER. *Curr. Protoc. Bioinforma.* **54,** 5.6.1-5.6.37 (2016).
30. Kozakov, D., Beglov, D., Bohnuud, T., Mottarella, S. E., Xia, B., Hall, D. R. & Vajda, S. How good is automated protein docking? *Proteins* **81,** 2159–66 (2013).
31. Higure, Y., Shimazaki, Y. & Nohmi, M. Can 4-chloro-m-cresol be substituted for caffeine as an activator of calcium oscillation in bullfrog sympathetic ganglion cells? *Cell Calcium* **39,** 467–70 (2006).
32. Hilgemann, D. W. Regulation and deregulation of cardiac Na+–Ca2+ exchange in giant excised sarcolemmal membrane patches. *Nature* **344,** 242–245 (1990).
33. Li, P. C., Yang, Y. C., Hwang, G. Y., Kao, L. Sen & Lin, C. Y. Inhibition of reverse-mode sodium-calcium exchanger activity and apoptosis by levosimendan in human cardiomyocyte progenitor cell-derived cardiomyocytes after anoxia and reoxygenation. *PLoS One* **9,** 1–9 (2014).
34. Meissner, G. Ryanodine activation and inhibition of the Ca2+ release channel of sarcoplasmic reticulum. *J. Biol. Chem.* **261,** 6300–6306 (1986).
35. Zimányi, I., Buck, E., Abramson, J. J., Mack, M. M. & Pessah, I. N. Ryanodine induces persistent inactivation of the Ca2+ release channel from skeletal muscle sarcoplasmic reticulum. *Mol. Pharmacol.* **42,** (1992).
36. Varro, A., Negretti, N., Hester, S. B. & Eisner, D. A. An estimate of the calcium content of the sarcoplasmic reticulum in rat ventricular myocytes. *Pflugers Arch.* **423,** 158–60 (1993).
37. Antoons, G., Mubagwa, K., Nevelsteen, I. & Sipido, K. R. Mechanisms underlying the frequency dependence of contraction and [Ca(2+)](i) transients in mouse ventricular myocytes. *J. Physiol.* **543,** 889–98 (2002).
38. Weber, C. R., Piacentino, V., Ginsburg, K. S., Houser, S. R. & Bers, D. M. Na+-Ca2+ exchange current and submembrane [Ca2+] during the cardiac action potential. *Circ. Res.* **90,**

182–189 (2002).
39. Thomas, N. L. & Williams, A. J. Pharmacology of ryanodine receptors and Ca 2+-induced Ca 2+ release. *WIREs Membr Transp Signal* **1,** 383–397 (2012).
40. Hartmann, N., Pabel, S., Herting, J., Schatter, F., Renner, A., Gummert, J., Schotola, H., Danner, B. C., Maier, L. S., Frey, N., Hasenfuss, G., Fischer, T. H. & Sossalla, S. Antiarrhythmic effects of dantrolene in human diseased cardiomyocytes. *Hear. Rhythm* **14,** 412–419 (2017).
41. Fiora, M., And, W.-G. & Isenberg, G. Total and free myoplasmic calcium during a contraction cycle: x-ray microanalysis in guinea-pig ventricular myocytes. *J. Physiol.* **435,** 349–372 (1991).
42. Ponsaerts, R., Wang, N., Himpens, B., Leybaert, L. & Bultynck, G. The contractile system as a negative regulator of the connexin 43 hemichannel. *Biol. Cell* **104,** 367–377 (2012).
43. Kondo, R. P., Weiss, J. N. & Goldhaber, J. I. Putative ryanodine receptors in the sarcolemma of ventricular myocytes. *Pflugers Arch. Eur. J. Physiol.* **440,** 125–131 (2000).
44. Kienitz, M. C., Bender, K., Dermietzel, R., Pott, L. & Zoidl, G. Pannexin 1 constitutes the large conductance cation channel of cardiac myocytes. *J. Biol. Chem.* **286,** 290–298 (2011).
45. Kontogeorgis, A., Li, X., Kang, E. Y., Feig, J. E., Ponzio, M., Kang, G., Kaba, R. A., Wit, A. L., Fisher, E. A., Morley, G. E., Peters, N. S., Coetzee, W. A. & Gutstein, D. E. Decreased connexin43 expression in the mouse heart potentiates pacing-induced remodeling of repolarizing currents. *Am J Physiol Hear. Circ Physiol* **295,** 1905–1916 (2008).
46. Beutner, G., Sharma, V. K., Lin, L., Ryu, S.-Y., Dirksen, R. T. & Sheu, S.-S. Type 1 ryanodine receptor in cardiac mitochondria: Transducer of excitation–metabolism coupling. *Biochim. Biophys. Acta - Biomembr.* **1717,** 1–10 (2005).
47. Jakob, R., Beutner, G., Sharma, V. K., Duan, Y., Gross, R. A., Hurst, S., Jhun, B. S., O-Uchi, J. & Sheu, S.-S. Molecular and functional identification of a mitochondrial ryanodine receptor in neurons. *Neurosci. Lett.* **575,** 7–12 (2014).
48. O-Uchi, J., Jhun, B. S., Hurst, S., Bisetto, S., Gross, P., Chen, M., Kettlewell, S., Park, J., Oyamada, H., Smith, G. L., Murayama, T. & Sheu, S.-S. Overexpression of ryanodine receptor type 1 enhances mitochondrial fragmentation and Ca 2-induced ATP production in cardiac H9c2 myoblasts. *Am J Physiol Hear. Circ Physiol* **305,** 1736–1751 (2013).
49. Jeyakumar, L. H., Gleaves, L. A., Ridley, B. D., Chang, P., Atkinson, J., Barnett, J. V. & Fleischer, S. The skeletal muscle ryanodine receptor isoform 1 is found at the intercalated discs in human and mouse hearts. *J. Muscle Res. Cell Motil.* **23,** 285–292 (2002).
50. Sorrentino, V. & Volpe, P. Ryanodine receptors: how many, where and why? *Trends Pharmacol. Sci.* **14,** 98–103 (1993).
51. Sutko, J. L. & Airey, J. A. Ryanodine receptor Ca2+ release channels: does diversity in form equal diversity in function? *Physiol. Rev.* **76,** 1027–71 (1996).
52. Sato, P. Y., Coombs, W., Lin, X., Nekrasova, O., Green, K. J., Isom, L. L., Taffet, S. M. & Delmar, M. Interactions between ankyrin-G, Plakophilin-2, and Connexin43 at the cardiac intercalated disc. *Circ. Res.* **109,** 193–201 (2011).
53. Yan, Z., Bai, X., Yan, C., Wu, J., Li, Z., Xie, T., Peng, W., Yin, C., Li, X., Scheres, S. H. W., Shi, Y. & Yan, N. Structure of the rabbit ryanodine receptor RyR1 at near-atomic resolution. *Nature* **517,** 50–55 (2015).
54. Sorgen, P. L., Duffy, H. S., Sahoo, P., Coombs, W., Delmar, M. & Spray, D. C. Structural changes in the carboxyl terminus of the gap junction protein connexin43 indicates signaling between binding domains for c-Src and zonula occludens-1. *J. Biol. Chem.* **279,** 54695–701 (2004).
55. Bennett, D. L., Cheek, T. R., Berridge, M. J., De Smedt, H., Parys, J. B., Missiaen, L. & Bootman, M. D. Expression and Function of Ryanodine Receptors in Nonexcitable Cells. *J Biol Chem. (11)6356-62.* **271,** (1996).
56. Guerrero, A., Fay, F. S. & Singer, J. J. Caffeine Activates a Ca2+-permeable, Nonselective Cation Channel in Smooth Muscle Cells. *J. Gen. Physiol.* **104,** 375–394 (1994).
57. Zhang, Y.-A., Tuft, R. A., Lifshitz, L. M., Fogarty, K. E., Singer, J. J. & Zou, H. Caffeine-activated large-conductance plasma membrane cation channels in cardiac myocytes: characteristics and significance. *Am. J. Physiol. Heart Circ. Physiol.* **293,** H2448-61 (2007).

58. Volk, T., Schwoerer, A. P., Thiessen, S., Schultz, J.-H. & Ehmke, H. A polycystin-2-like large conductance cation channel in rat left ventricular myocytes. *Cardiovasc. Res.* **58,** 76–88 (2003).
59. Hirst-Jensen, B. J., Sahoo, P., Kieken, F., Delmar, M. & Sorgen, P. L. Characterization of the pH-dependent Interaction between the Gap Junction Protein Connexin43 Carboxyl Terminus and Cytoplasmic Loop Domains. *J Biol Chem. (8)5801-13.* **282,** (2007).
60. Leybaert, L., Lampe, P. D., Dhein, S., Kwak, B. R., Ferdinandy, P., Beyer, E. C., Laird, D. W., Naus, C. C., Green, C. R. & Schulz, R. Connexins in Cardiovascular and Neurovascular Health and Disease: Pharmacological Implications. *Pharmacol. Rev. Pharmacol Rev* **69,** 396–478 (2017).
61. Iyyathurai, J., Wang, N., Catheleyne D'hondt, Jiang, J. X., Luc Leybaert, · & Bultynck, · Geert. The SH3-binding domain of Cx43 participates in loop/tail interactions critical for Cx43-hemichannel activity. *Cell. Mol. Life Sci.* **75,** 2059–2073 (2018).
62. Lübkemeier, I., Requardt, R. P., Lin, X., Charney, L. H., Sasse, P., Andrié, R., Schrickel, J. W., Chkourko, H., Bukauskas, F. F., Purpura, D. P., Kim, J.-S., Frank, M., Malan, D. & Zhang, J. Deletion of the last five C-terminal amino acid residues of connexin43 leads to lethal ventricular arrhythmias in mice without affecting coupling via gap junction channels. *Basic Res Cardiol* **108,** 348 (2013).
63. Belevych, A. E., Terentyev, D., Terentyeva, R., Ho, H.-T., Gyorke, I., Bonilla, I. M., Carnes, C. A., Billman, G. E. & Györke, S. Shortened Ca 2+ Signaling Refractoriness Underlies Cellular Arrhythmogenesis in a Postinfarction Model of Sudden Cardiac Death. *Circ Res* **110,** 569–577 (2012).
64. Vandersickel, N., Kazbanov, I. V., Nuitermans, A., Weise, L. D., Pandit, R. & Panfilov, A. V. A study of early afterdepolarizations in a model for human ventricular tissue. *PLoS One* **9,** (1):e84595 (2014).
65. Verkerk, A. O., Tan, H. L., Kirkels, J. H. & Ravesloot, J. H. Role of Ca2+-activated Cl-current during proarrhythmic early afterdepolarizations in sheep and human ventricular myocytes. *Acta Physiol. Scand.* **179,** 143–148 (2003).
66. Campos, F. O., Shiferaw, Y., Prassl, A. J., Boyle, P. M., Vigmond, E. J. & Plank, G. Stochastic spontaneous calcium release events trigger premature ventricular complexes by overcoming electrotonic load. *Cardiovasc Res. (1)175-83.* **107,** (2015).
67. Asp, M. L., Martindale, J. J., Heinis, F. I., Wang, W. & Metzger, J. M. Calcium mishandling in diastolic dysfunction: mechanisms and potential therapies. *Biochim. Biophys. Acta* **1833,** 895–900 (2013).
68. Chelu, M. G. & Wehrens, X. H. T. Sarcoplasmic reticulum calcium leak and cardiac arrhythmias. *Biochem. Soc. Trans.* **35,** 952–6 (2007).
69. Selby, D. E., Palmer, B. M., Lewinter, M. M. & Meyer, M. Tachycardia-induced Diastolic Dysfunction and Resting Tone in Myocardium from Patients with Normal Ejection Fraction. *J Am Coll Cardiol* **58,** (2): 147–154. (2011).
70. Zissimopoulos, S., Seifan, S., Maxwell, C., Williams, A. J. & Lai, F. A. Disparities in the association of the ryanodine receptor and the FK506-binding proteins in mammalian heart. *J. Cell Sci.* **125,** 1759–69 (2012).
71. Li, J., Imtiaz, M. S., Beard, N. A., Dulhunty, A. F., Thorne, R., vanHelden, D. F. & Laver, D. R. ß-Adrenergic Stimulation Increases RyR2 Activity via Intracellular Ca2+ and Mg2+ Regulation. *PLoS One* **8,** e58334 (2013).

Table 1. Electrical properties of ventricular action potentials in $Cx43^{fl/fl}$ control and $Cx43^{Cre\text{-}ER(T)/fl}$ Cx43 knock-down mice

Condition	n	MDP (mV)	APA (mV)	APD_{50} (msec)	APD_{70} (msec)	APD_{90} (msec)
$Cx43^{fl/fl}$ control	10	-78.56 ± 1.47	76.07 ± 3.63	18.17 ± 1.62	23.84 ± 1.94	57.97 ± 4.99
$Cx43^{fl/fl}$ + RyRHCIp	6	-75.29 ± 0.43	81.47 ± 6.29	18.85 ± 2.64	29.52 ± 4.74	78.15 ± 7.00 #
$Cx43^{fl/fl}$ + ScrRyRHCIp	6	-75.19 ± 1.07	73.08 ± 4.93	15.79 ± 1.96	21.40 ± 2.72	62.50 ± 6.57
$Cx43^{Cre\text{-}ER(T)/fl}$ Cx43 KD	7	-78.38 ± 2.01	88.13 ± 7.55	11.58 ± 1.32 *	16.77 ± 1.60	53.03 ± 5.87

MDP, indicates maximal diastolic potential; APA, action potential amplitude and APD, action potential duration. *P* values refer to difference between Cx43fl/fl control and the tested condition. * $P = 0.013$ and # $P = 0.022$ (N = 6; one-way ANOVA, Bonferroni posttest).

Table 2. Two modes of Cx43 hemichannel activation

Combined RyR/$[Ca^{2+}]_i$ activation at resting potential	Electrical activation by stepping to positive voltages
Fast spiking channel openings lasting ~9 msec	Long channel openings lasting 100 msec up to 2 sec
Inhibited by RyRHCIp	Not affected by RyRHCIp

Figure legends:

Fig. 1. Effect of RyR activation in ventricular cardiomyocytes held at resting membrane potential. a. Example traces showing unitary current events triggered by RyR agonists at V_h = -70 mV. The expanded traces in red were obtained after subtraction of the macroscopic current, which is mainly carried by the electrogenic NCX transporter.
b. Transition event histograms of the red traces shown in (a), illustrating a ~220 pS unitary conductance. O_1, O_2, O_3 indicate 220, 440 and 660 pS respectively.
c. Representative recording of an experiment under low extracellular Na^+ conditions applied to reverse the NCX transporter mode resulting in intracellular Ca^{2+} elevation. Ryanodine (100 µM) was added to the pipette solution to keep RyRs closed during recordings. The current trace shown below displayed no signs of unitary activity under those conditions.
d. All-point histogram of the current trace depicted in (c), showing absence of 220 pS unitary activity.

Fig. 2. Combined RyR activation/$[Ca^{2+}]_i$ elevation is necessary to trigger unitary current activity.
a. Repeated caffeine exposure triggers unitary activity at the first but not at the second application.
b. Under conditions of $[Ca^{2+}]_i$ clamping to 250 nM (10 mM BAPTA), repeated RyR activation invariably provoked subsequent activation of unitary current activities. In between caffeine applications, 250 nM $[Ca^{2+}]_i$ by itself was not sufficient to trigger unitary current activity.
c. Representative current traces depicting unitary current activities obtained upon caffeine applications at different $[Ca^{2+}]_i$. RyR activation with $[Ca^{2+}]_i$ set at 50 nM did not trigger unitary current activity, which only appeared upon elevating $[Ca^{2+}]_i$. The red traces represent associated $[Ca^{2+}]_i$ recordings, illustrating stable $[Ca^{2+}]_i$ clamping. $[Ca^{2+}]_i$ shown are calculated values; see text for the corresponding measured values.
d. Transition event histograms of each recording shown in (c). At 500 nM $[Ca^{2+}]_i$, increased HC opening activity can be clearly inferred from the increased frequency of double (O_2) and triple (O_3) stacked channel openings and corresponding conductance states, while further elevation to 1 µM reduced HC activity.
e. Average data of unitary current integration over time representing membrane charge transfer (Q_m) in the presence of various $[Ca^{2+}]_i$ levels (50 nM n = 5, 250 nM n = 10, 500 nM n = 8, 1 µM n = 6; N = 5). RyR activation at 50 nM clamped $[Ca^{2+}]_i$ does not activate HC opening while increasing $[Ca^{2+}]_i$ to 250 and 500 nM gradually increases the opening response. $[Ca^{2+}]_i$ 250 nM versus 50 nM P = 0.007 (unpaired Student's t-test). $[Ca^{2+}]_i$ 250 nM versus 500 nM P = 0.0187; 1 µM versus 500 nM P = 0.023 (one-way ANOVA, Bonferroni posttest).
f. Examples of current traces triggered by combined RyR activation and 250 nM $[Ca^{2+}]_i$ at different membrane potentials. While negative potentials showed spiking unitary activities, positive potentials were characterized by much longer lasting outward currents associated with channel opening.
g. Current-voltage plot based on the traces shown in (f), illustrating a slope conductance of 230 ± 2.8 pS and a reversal potential close to 0 mV, indicating involvement of a poorly selective channel (n = 10; N = 4).

Fig. 3. Unitary current activity is largely reduced in cardiomyocytes isolated from Cx43 knockdown mice.
a. Example current traces (black) and $[Ca^{2+}]_i$ levels (red) showing the difference between control $Cx43^{fl/fl}$ animals and Cx43 knockdown in $Cx43^{Cre\text{-}ER(T)/fl}$ animals, both treated with tamoxifen.

b. Western blot and relative quantification illustrating Cx43 protein levels in ventricular samples isolated from tamoxifen treated $Cx43^{fl/fl}$ and $Cx43^{Cre\text{-}ER(T)/fl}$ animals (n = 3; N = 3). *P* = 0.002 versus $Cx43^{fl/fl}$ (unpaired Student's t-test).
c. Summary Q_m data illustrating significantly reduced unitary current activity in ventricular cardiomyocytes from $Cx43^{Cre\text{-}ER(T)/fl}$ animals ($Cx43^{fl/fl}$ 50 nM $[Ca^{2+}]_i$ n = 7, $Cx43^{fl/fl}$ 250 nM $[Ca^{2+}]_i$ n = 20, $Cx43^{Cre\text{-}ER(T)/fl}$ 50 nM $[Ca^{2+}]_i$ n = 10, $Cx43^{Cre\text{-}ER(T)/fl}$ 250 nM n = 12; N = 4). $Cx43^{fl/fl}$ 250 nM versus $Cx43^{Cre\text{-}ER(T)/fl}$ 250 nM $[Ca^{2+}]_i$ *P* = 0.0021; $Cx43^{fl/fl}$ 50 nM versus $Cx43^{fl/fl}$ 250 nM $[Ca^{2+}]_i$ *P* = 0.0012 (one-way ANOVA, Bonferroni posttest).

Fig. 4. Cx43 colocalizes with RyR2 at the IDs of cardiomyocytes.
a. Cx43 (green) and RyR2 (red) immunocytochemistry of isolated ventricular cardiomyocytes. Colocalization analysis by Manders coefficient quantification indicated that 24.49 ± 3.46 % of the Cx43 signal overlapped with the RyR2 signal (n = 8; N = 3).
b. Cardiac ventricular cryosections were used for proximity ligation assays to study RyR2-Cx43 approximation (red signal) at the intercalated disc marked by immunostaining for the structural protein cadherin (white signal).
c. Proximity ligation assays using two Cx43 antibodies with different epitopes was used as positive control. White dashed insets delineate zoomed regions of interest. Arrows indicate clearly observable colocalization spots depicted as red dots (proximity ligation signal) on white cadherin signal. Scale bars, 10 µm.

Fig. 5. Cx43 interacts with RyR2 in cardiomyocytes.
Co-IP and *in silico* studies of possible interaction sites between Cx43 and RyR2.
a. Co-IP assays on whole heart (left column) and isolated cardiomyocytes lysates (right column). Cx43 co-precipitated with RyR2; N-cadherin was used as a positive control (N = 3). The second ~400 KDa RyR2 band has been reported to correspond to the C-terminal fraction of the channel [70,71].
b. Structure of rabbit RyR1 (PDB: 3J8H; left panel) and the homology model of mouse RyR2 cytoplasmic domain used for the docking study (1-2905; right panel): N-terminal domain (NTD) in yellow, SPRY1 domain in gray, P1 domain in orange, SPRY2 domain in violet and SPRY3 domain in dark red, handle region in teal blue and helical region in lime green. The interaction sequences are reported in the table.
c. Membrane topology of Cx43 with indication of the predicted binding region of the RyRHCIp mimetic peptide on the C-terminal tail (CT) (green). The sequence partly overlaps with a second α-helical CT domain (yellow).

Fig. 6. RyRHCIp inhibits HC activity triggered in cardiomyocytes and affects ventricular action potential, while it has no effect on electrically triggered HC currents in HeLa Cx43 cells.
a. Time course of RyRHCIp inhibition of Cx43 HC unitary currents activated by RyR/$[Ca^{2+}]_i$ elevation in cardiomyocytes. Q_m values were normalized relative to the value at the 30 s timepoint for each condition. RyRHCIp (250 µM) significantly decreased Cx43 HC opening activity (red), while scrambled RyRHCIp (ScrRyRHCIp; 250 µM; blue) had no effect (Control 250 nM $[Ca^{2+}]_i$ n = 11, RyRHCIp n = 9, ScrRyRHCIp n = 9; N = 5). Timepoint 120 sec *P* = 0.0008, 150 sec *P* = 0.00003, 180 sec *P* = 0.00006, 210, 240, 270 and 300 sec *P* = <0.00001 versus t = 30 s (paired Student's t-test).

b. Summary graph of non-normalized Q_m data at 30 and 300 s (Control 250 nM $[Ca^{2+}]_i$ n = 11, RyRHCIp n = 9, ScrRyRHCIp n = 9; N = 5). RyRHCIp $P = 0.0005$, $P = 0.040$ versus control and ScrRyRHCIp respectively (one-way ANOVA, Bonferroni posttest).
c. Example current traces recorded in HeLa Cx43 cells in the absence or presence of RyRHCIp (250 µM). Voltage steps to +70 mV were applied to induce Cx43 HC activity.
d. All-point histograms of each set of recordings depicted in (c).
e. Summary Q_m data demonstrating no effect of RyRHCIp on Cx43 HC activity in HeLa Cx43 cells (control n = 18, RyRHCIp n = 20; N = 4).
f. Current clamp recordings of action potentials in cardiomyocytes, demonstrating the effect of Cx43 knockdown in $Cx43^{Cre\text{-}ER(T)/fl}$ mice and of RyRHCIp (250 µM) compared to measurements in $Cx43^{fl/fl}$ control mice (values see Table 1).

Fig. 7. Schematic model summarizing the findings of this study.
a. RyR2 and Cx43 interact and keep the channel in a closed state by preventing loop-tail interaction.
b. Activation of RyR2 facilitates loop-tail interaction (CT-CL) thereby bringing the channel in a closed but available to open state.
c. $[Ca^{2+}]_i$ elevation triggers the actual opening of Cx43 HCs.
d. RyRHCIp competes with RyR2 for binding to the Cx43 CT domain, thereby bringing the channel in a stabilized closed state.

Fig. 1

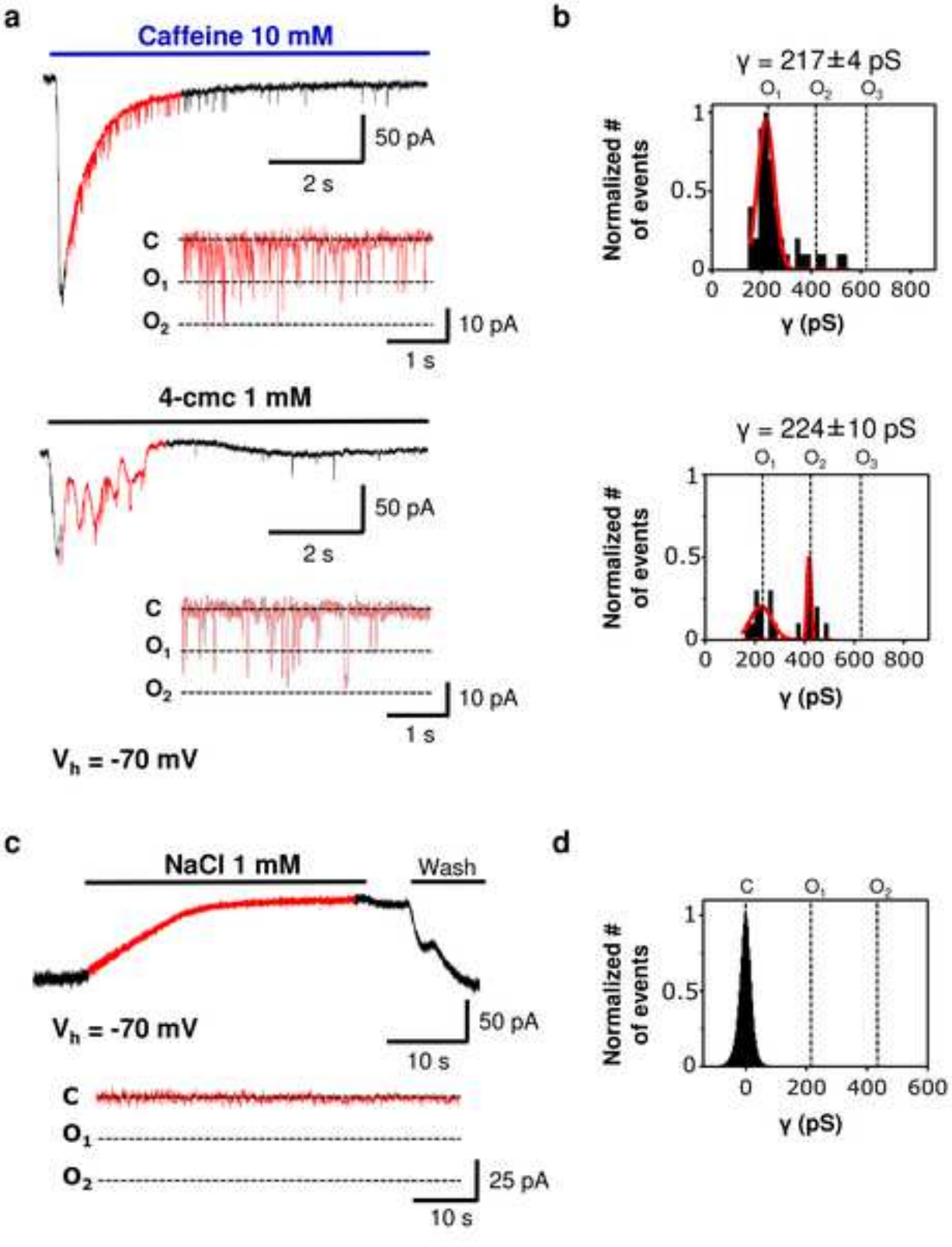

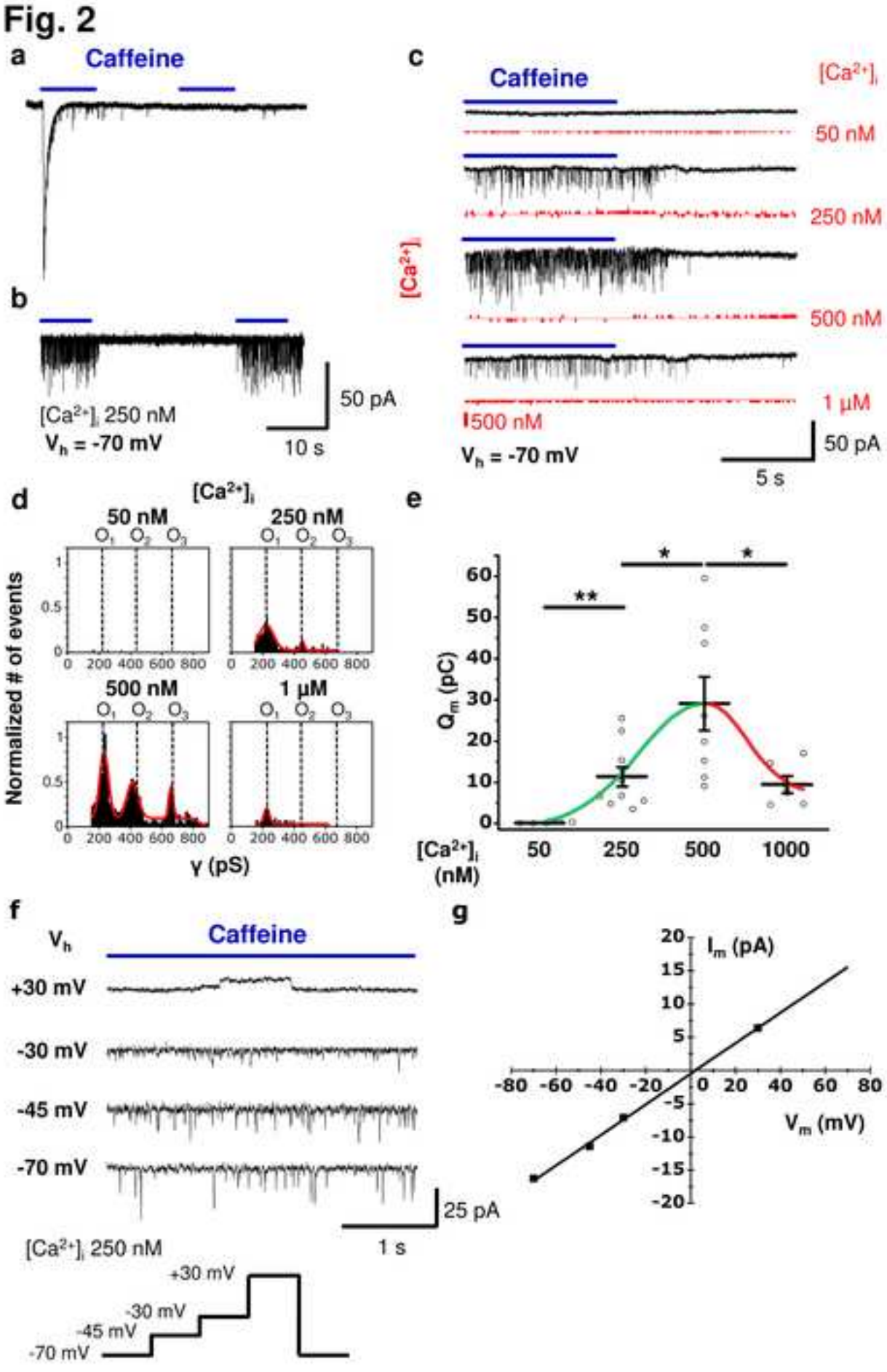

Fig. 3

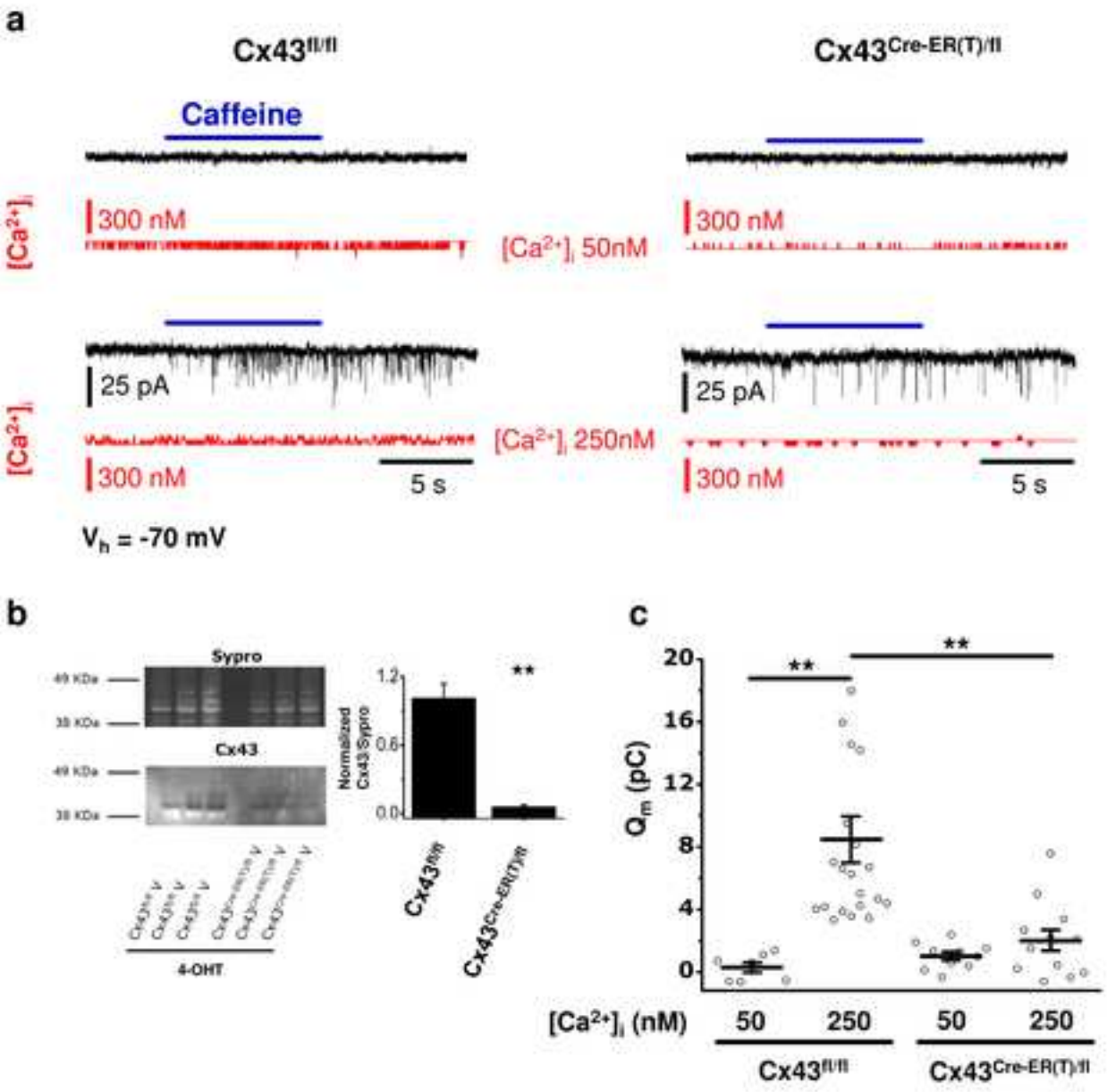

Figure 4

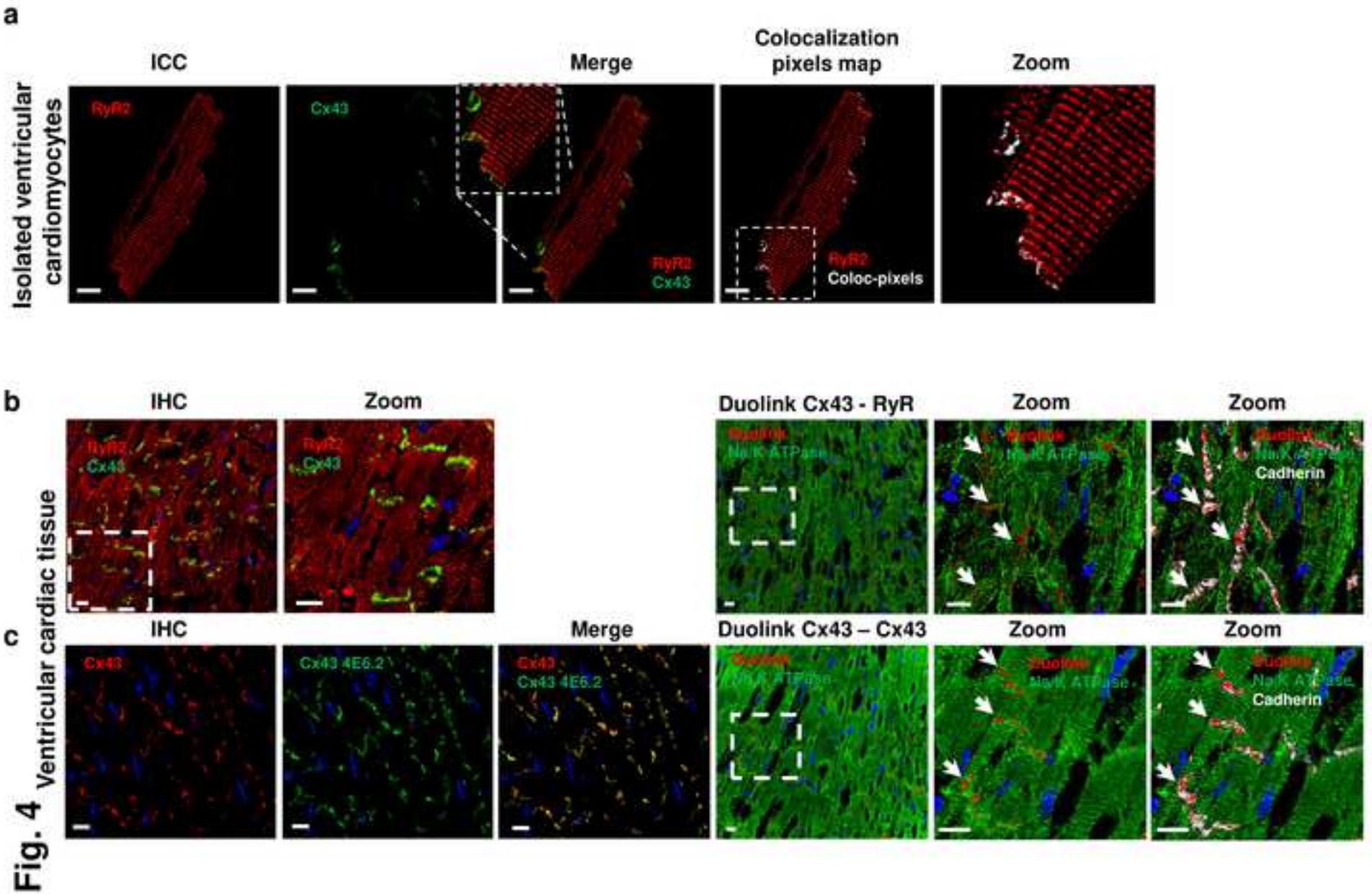

Fig. 4

Fig. 5

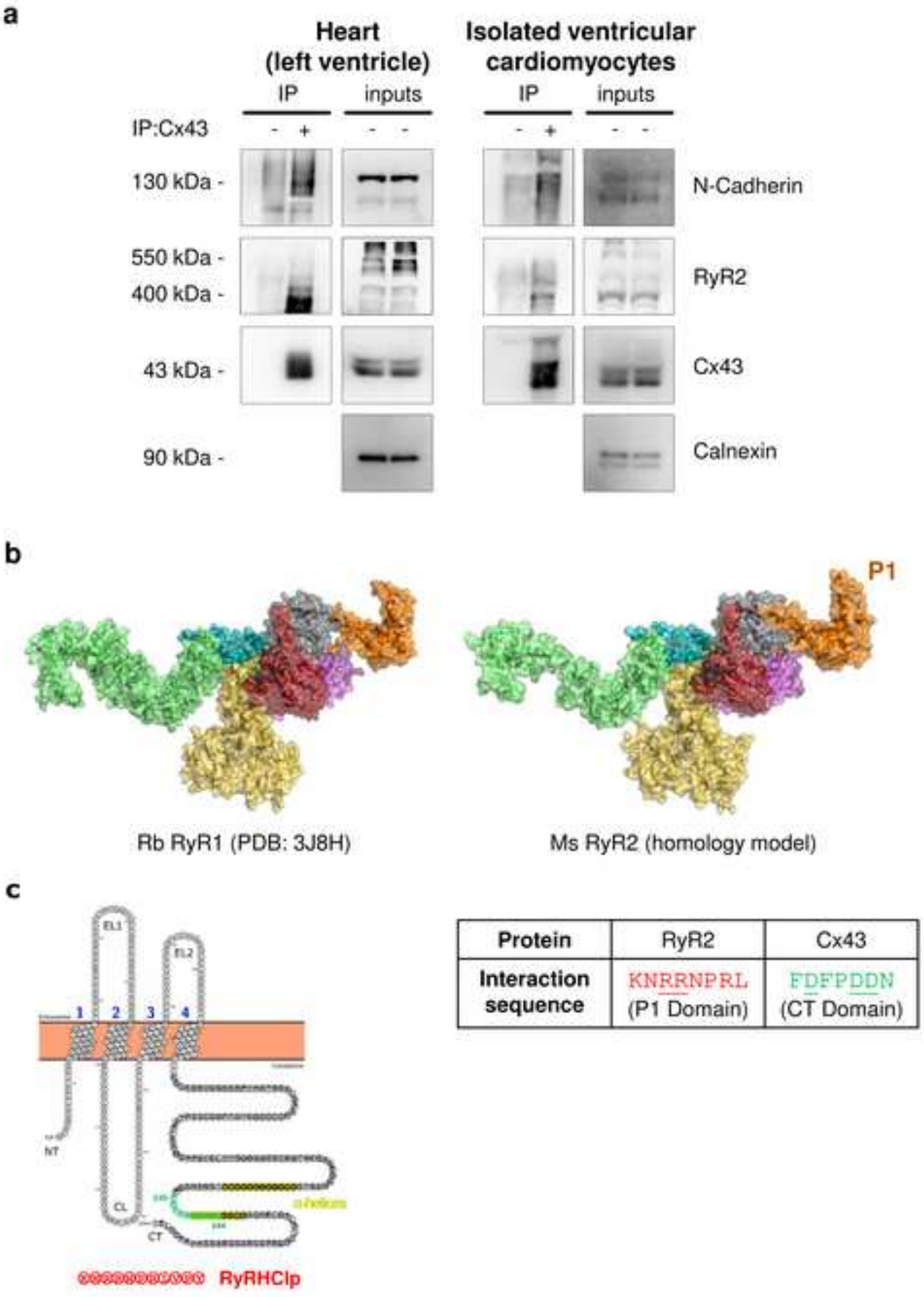

Protein	RyR2	Cx43
Interaction sequence	KNRRNPRL (P1 Domain)	FDFPDDN (CT Domain)

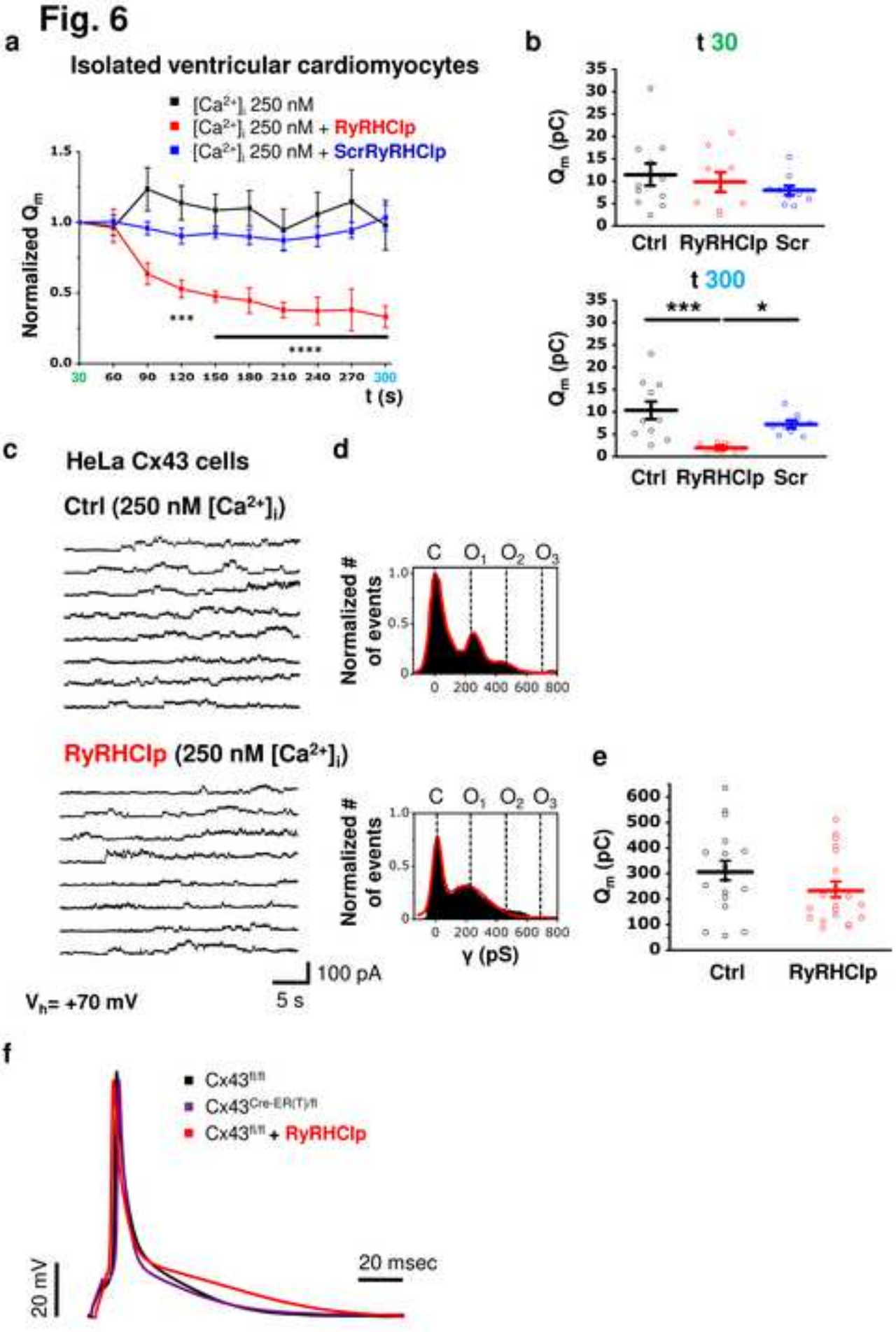

Fig. 7

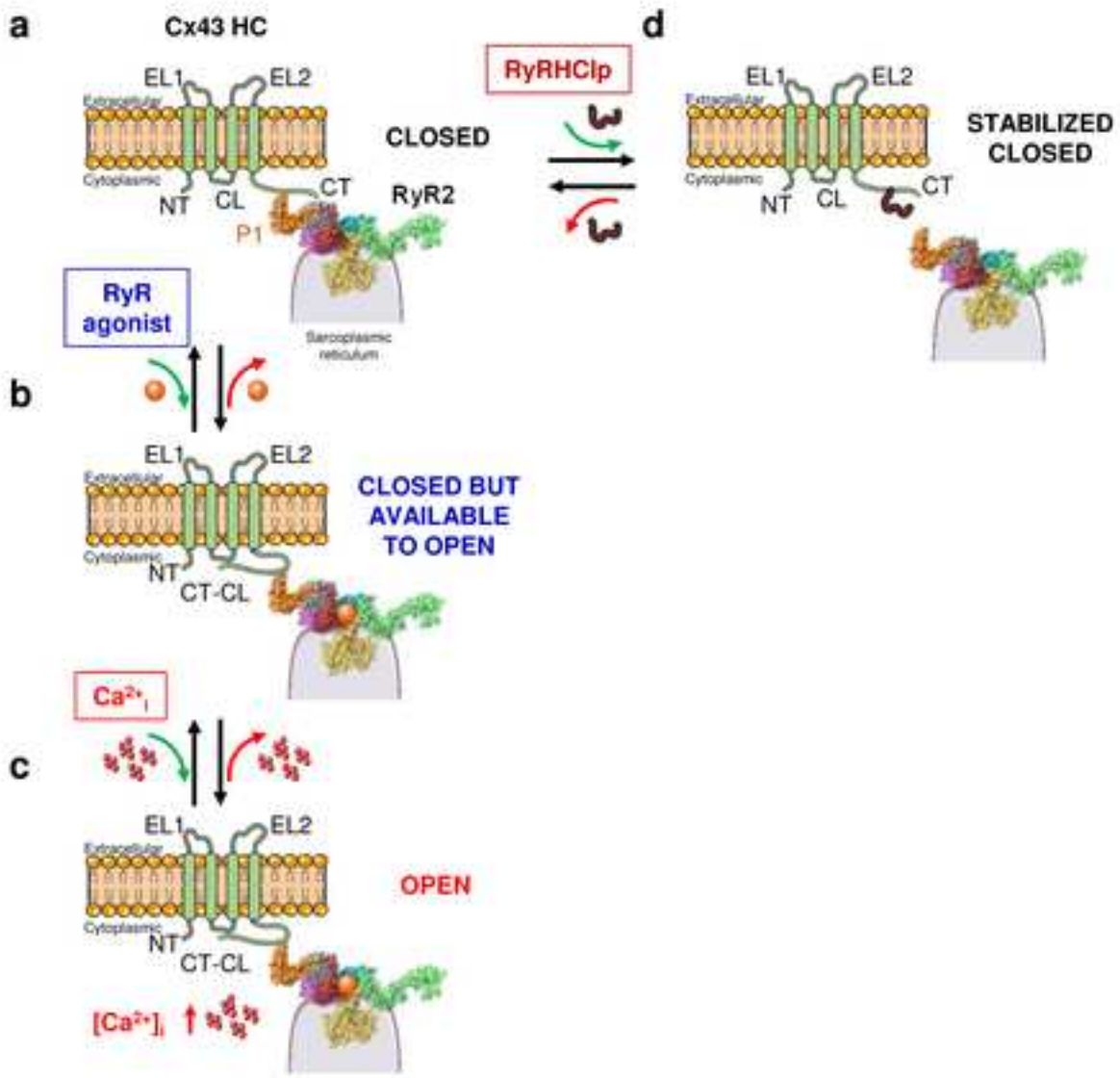

Graphical Abstract